*Acta Oceanol. Sin.*, 2018, Vol. 37, No. 9, P. 29–40
DOI: 10.1007/s13131-018-1263-8
http://www.hyxb.org.cn
E-mail: hyxbe@263.net

# A numerical study on the effect of tidal flat's slope on tidal dynamics in the Xiangshan Bay, China

LI Li[1, 2], YE Taoyan[1], HE Zhiguo[1, 2], XIA Yuezhang[1, 2*]

[1] Ocean College, Zhejiang University, Zhoushan 316021, China

[2] State Key Laboratory of Satellite Ocean Environment Dynamics, Second Institute of Oceanography, State Oceanic Administration, Hangzhou 310058, China

Received 18 October 2017; accepted 19 December 2017

© Chinese Society for Oceanography and Springer-Verlag GmbH Germany, part of Springer Nature 2018

**Abstract**

The Xiangshan Bay is a semi-enclosed and narrow bay, which is characterized by large scale tidal flats and has been historically utilized through coastal construction and aquaculture engineering. The hydrodynamic model using the Finite Volume Coastal Ocean Model (FVCOM) was constructed to examine the changes of tidal dynamics due to the variation of tidal flat slopes. According to the model results, a decreased slope of a tidal flat would amplify the $M_2$ tidal amplitude and delay the $M_2$ tidal phase in the inner harbor, due to an increased tidal prism, and vice versa. The amplitude of the main shallow-water tide $M_4$ would be amplified/dampened in the entire bay due to the changed bottom friction, if the tidal flat's slope were reduced/increased at the Tie inlet. The phase was advanced. The change of a tidal flat's slope at the Tie inlet had greater impacts on tidal amplitude, phase and duration asymmetry, than that at the Xihu inlet. The impact of changes of the tidal flat slope at the Xihu inlet was small and was constrained locally. Changes in the tidal flats' slopes at the Tie and Xihu inlets changed the tidal duration asymmetry, residual current and tidal energy via modulating tides. The ebb dominance decreased when the tidal flat's slope at the Tie inlet was changed. Decreased/increased ebb dominance occurred when the tidal flat's slope was reduced/increased at the Xihu inlet. The residual current and tidal energy density was amplified/dampened and more/less tidal energy was dissipated, with reduced/increased slope at both of the inlets. The findings in this study are instructive to coastal engineering and estuarine management.

**Key words:** tidal flat's slope, tidal dynamics, tidal asymmetry, tidal energy, Xiangshan Bay

**Citation:** Li Li, Ye Taoyan, He Zhiguo, Xia Yuezhang. 2018. A numerical study on the effect of tidal flat's slope on tidal dynamics in the Xiangshan Bay, China. Acta Oceanologica Sinica, 37(9): 29–40, doi: 10.1007/s13131-018-1263-8

## 1 Introduction

A tidal flat's slope can change local hydrodynamics and bottom stress (Franz et al., 2014; Shi et al., 2012). Hence, it is fundamental to study the response of tides to changes in a tidal flat's slope at a macro-tidal estuary with a large tidal flat area in order to understand its transport properties, such as sediment transport, and to develop bay planning, such as port construction (Rees et al., 2014). In particular, the mechanics of sediment transport can determine the fate of a bay's morphology, the siltation or erosion pattern of a navigation channel and the generation of a turbid zone (Jiang et al., 2013).

The reduction of tidal flat areas modulates the tidal characteristics (Friedrichs and Aubrey, 1994; Friedrichs and Madsen 1992), including the amplitude and phase of the tidal constituents, particularly the shallow water tides, through modulating bottom dissipation and advection processes in the tidal flat areas. Consequently, the tidal duration asymmetry is changed, such as in the Darwin Harbour, Australia and Jiaozhou Bay, China (Li et al., 2012; Gao et al., 2014). The loss of tidal flat areas increases flood dominance in the Xiangshan Bay (Li et al., 2017). Large-scale reclamation of tidal flats in the Bohai Sea, Yellow Sea and East China Sea has increased the tidal amplitude and onshore sediment transport (Song et al., 2013). The reduction of tidal flat areas changes the suspended sediment concentration and net sediment fluxes through modulating tides and tidal duration asymmetry. The formation mechanism of estuarine turbidity maxima (ETM) is consequently changed. For example, the tidal pumping effect is one of the most important factors in forming the ETM in the Changjiang Estuary (Li et al., 2016). More sediment is pumped landward in the Darwin Harbour (Li et al., 2014) and Jiaozhou Bay changes from erosion to siltation (Gao et al., 2017), due to the increased tidal pumping effect caused by the loss of tidal flat areas.

The Xiangshan Bay is a semi-enclosed bay situated in a northeast-southwest direction, with scattered islands distributed in and out of the bay (Fig. 1a). The bay is 60 km long from the mouth to the upper head. Its width shrinks from about 18 km at the mouth to about 4 km near the mouth of the Xihu inlet. It is a deep water shelter with an average depth of 10 m and large tidal flats over more than 30% of its water area (563 km$^2$) (Dong and Su, 1999a). The tidal flats' slopes around the Tie inlet and the Xihu inlet are about 1/600 and 1/400, respectively. The slopes were

Foundation item: The National Natural Science Foundation of China under contract No. 41606103; the Zhejiang Provincial Natural Science Foundation of China under contract Nos LQ16D060002 and LR16E090001; the State Key Laboratory of Satellite Ocean Environment Dynamics (Second Institute of Oceanography, State Oceanic Administration) under contract No. SOED1512; the National Key Research and Development Program of China under contract No. 2017YFC1405101.
*Corresponding author, E-mail: yzxia@zju.edu.cn

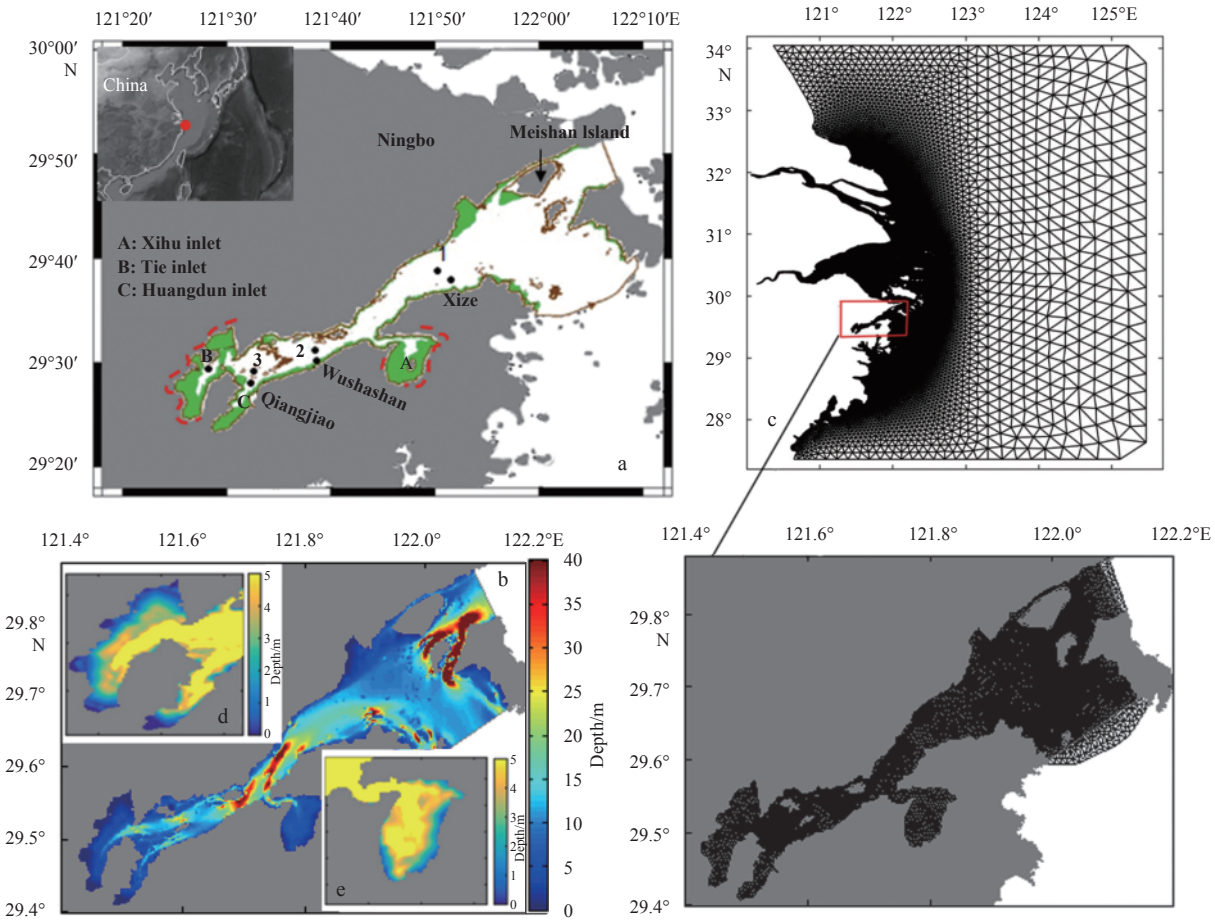


**Fig. 1.** Map of the Xiangshan Bay. a. Model domain and observation stations of the Xianshan Bay, elevation data were collected from the three stations of Xize, Wushashan and Qiangjiao, current data were collected at Stas 1, 2 and 3; b. depth of the model domain, positive value indicates downward, shading for water depth is with respect to the mean surface level in 2003; c. model grids; d. the water depth in the Tie inlet; and e. the water depth in the Xihu inlet.

calculated by the ratio of the vertical distance to the horizontal distance, of the 0 m and 5 m water depth contour. The average annual wave height is only 0.4 m in the outer bay. There are three inlets, the Xihu inlet, the Tie inlet and the Huangdun inlet. Rivers running into the bay are smaller than around the tidal prism of Xiangshan Bay. Tides in Xiangshan Bay are semi-diurnal with maximum tidal ranges of about 6.5 m when tides propagate towards the bay head (Xu et al., 2014). Compared with other factors, tides dominate the sedimentation processes in Xiangshan Bay (Gao et al., 1990). Many studies have been carried out on tides in a bay, to understand tidal exchange (Azofra et al., 2014; Chen and Su, 1999; Cai et al., 1985), tidal response time and deformation (Dong and Su, 1999a, 1999b; Ksanfomality et al., 1997; Mishra et al., 2015; Seo et al., 2015).

With the development of the marine economy and coastal engineering around the Xiangshan Bay, claiming new land from the sea has become a potential way to satisfy the demand (Niu and Yu, 2008). As a result, a number of natural tidal flats have been lost or modified. The slopes of natural tidal flats are between 1/100 and 1.6/100 (Lee et al., 1998). The constructed coastlines have changed the tidal flats' areas and slopes. Around the Xiangshan Bay, about 42 km$^2$ land was reclaimed from the sea by 2003, and another 35 km$^2$ land was reclaimed by 2010 (Zeng et al., 2011). Similarly, the tidal flat in the Changjiang Estuary was also claimed as land or accreted due to sediment erosion from the subaqueous delta (Zhu et al., 2016). Changes in tidal flats impact the characteristics of tidal asymmetry through modulating tides, and consequently affect the transport of nutrients, pollutants and sediment, which determine the erosion and deposition pattern of a bay. Therefore, some tidal flats have been reconstructed to restore previous damage and to create artificial tidal flats to mitigate lost functions (Lee et al., 1998; Montalto et al., 2006), e.g., tidal flats at the south coast of the Hangzhou Bay. Research has been done on the effects of reduced tidal flat areas, e.g., impact of reclamation on hydrodynamics.

On the contrary, dredging and sand mining in estuaries is another way to satisfy fast developing urban construction and port development (Trop, 2017; Uścinowicz et al., 2014), and this has caused a reduction of the tidal flat elevation. Dredging is usually done to deepen navigational channels. However, the deepened channels can be partly refilled by re-suspended sediment from the vicinity, thereby inducing subaqueous deltas and tidal flat erosion (Dallas and Barnard, 2011). Sand mining has often meant sand being removed from sandbars, or even directly from tidal flats. At the mouth of Xiangshan Bay, a reduction of the sand beach elevation of the Qitou Estuary occurred and the tidal currents were impacted due to sand mining (Jin et al., 2006). A loss of sand can induce bathymetry change and coastal erosion, as occurred in Xiamen (Chen and Cai, 2001) and the Shandong Peninsula (Gao and Han, 2003).

The reduced/increased tidal flat slopes around the Tie inlet impact on the tides and tidal duration asymmetry in the bay (Li et al., 2017). However, the impacts of tidal flat slope changes by different degrees and in different locations on tidal dynamics still needs further examination to help tidal flat restoration and biological-environmental management of tidal flats.

The primary aims of this study are to build and calibrate a hydrodynamic model of the Xiangshan Bay using field survey data collected by the State Key Laboratory of Satellite Ocean Environment Dynamics (SOED). We then use the numerical model to examine the impacts of changes in tidal flat's slope on the tidal dynamics in bays. The results in this study can be used for sediment and pollutant transport research in the near future.

## 2 Methods

The numerical model FVCOM and the calculation of tidal asymmetry are described in this section. The model calibration is conducted via comparing modeled and observed tidal elevations and currents.

### 2.1 *Model description*

The Finite Volume Coastal Ocean Model (FVCOM) (Chen et al., 2003) is a three-dimensional hydrodynamic model. The unstructured grid used by FVCOM is especially suited to study the Xiangshan Bay, which has a complex shoreline geometry and dynamic physical processes. FVCOM solves the three-dimensional momentum, continuity and density equations using a finite-volume method to allow mass conservation to be strictly maintained. The continuity equation is

$$\frac{\partial \zeta}{\partial t}+\frac{\partial (Du)}{\partial x}+\frac{\partial (Dv)}{\partial y}+\frac{\partial w}{\partial \sigma}=0, \tag{1}$$

where $\zeta$ is the height of the free surface; $D$ is the total water column depth; $x$, $y$ and $\sigma$ are the eastward, northward and vertical coordinates, respectively; $u$, $v$ and $w$ are the corresponding velocity components. The model employs the Mellor-Yamada level-2.5 turbulence closure scheme (Mellor and Yamada, 1982) for vertical mixing, and uses the Smagorinsky scheme for horizontal mixing (Smagorinsky, 1963). The drag coefficient $C_{\rm d}$ is assigned as 0.000 3 in the bay according to field observation (Xu et al., 2014). The drag coefficient $C_{\rm d}$ of the ESC domain is determined by matching a logarithmic bottom layer to the model at a height $z_{\rm ab}$ above the bottom,

$$C_{\rm d}=\max\left(\frac{\kappa^2}{\left(\ln(z_{\rm ab}/z_0)\right)^2},\ 0.000\ 3\right), \tag{2}$$

where $\kappa$=0.4 is the von Karman constant and $z_0$ is the bottom roughness parameter (FVCOM User Manual, 2006). Inside the Xiangshan Bay, the bottom drag coefficient is set as $0.3\times10^{-3}$ according to ADCP data (Xu et al., 2014).

### 2.2 *Model configuration*

#### 2.2.1 *Domain*

The model domain covers the entire East China Sea with a model grid consisting of about 50 000 elements and 28 000 nodes in the horizontal plane. The small domain of Xiangshan Bay (Fig. 1a) was nested into the ECS domain (Fig. 1c). The bay geometry and water depth, which is based on all the available bathymetry and shoreline data collected by the Key State Laboratory of Satellite Ocean Environment Dynamics (SOED), relate to the mean surface level as shown in Fig. 1b. The cell sizes of the domain range from 30 m near the islands to 2 000 m at the bay mouth. To accurately resolve the vertical profiles of currents, we specified 6 vertical layers in the water column using the $\sigma$-coordinate system.

Three stations, Qiangjiao, Wushashan and Xize collected elevation data, and these are indicated in Fig. 1a. Also indicated are Stas 1, 2 and 3 for collecting current observations in accordance with the respective elevation stations.

#### 2.2.2 *Boundary conditions and forcing*

The open boundary is located far away from the bay mouth (Fig. 1c). The open-boundary condition for water level is specified using tidal elevations predicted by the TPXO7.2 global model of ocean tides (http://volkov.oce.orst.edu/tides/TPXO7.2.html). An hourly tidal elevation is applied to the open-ocean boundary, which is constructed using four diurnal components ($K_1$, $O_1$, $P_1$ and $Q_1$), four semi-diurnal components ($M_2$, $S_2$, $N_2$ and $K_2$), three shallow-water components ($M_4$, $MS_4$ and $MN_4$), and two long-period components ($M_f$ and $M_m$).

The runoff into the bay is small, compared to the tidal prism and tidal range in the bay. There are no large rivers discharging into the bay (Gao et al., 1990). Wind has often been considered a predominant driving force for sediment re-suspension in many estuaries, especially the shallow ones (Wright et al., 1992). Given that the maximum and mean tidal ranges in the Xiangshan Bay are 5.6 and 3.1 m, respectively, the hydrodynamics in the bay are expected to be driven mainly by tidal currents. Therefore, both wind and heat fluxes at the free-surface boundary are neglected in our model.

#### 2.2.3 *Initial conditions*

The model was initialized with a constant salinity of 23 and with a constant temperature of 25°C, which are the typical mean values in the bay during the study period of winter. The model was integrated for 60 days from 7 November 2003, during which time station data were available for validation. The key parameters of the model are summarized in Table 1.

#### 2.2.4 *Model runs*

In order to check the response of tidal dynamics to changes in the slope of a tidal flat, 13 numerical experiments were designed.

**Table 1.** Key model parameters

| Model parameter | Value |
|---|---|
| Model time setup | 1.0 s |
| Bottom friction coefficient | calculated according to Eq. (2) in the ECS domain; set as $0.3\times10^{-3}$ inside the bay |
| Horizontal diffusion | Smagorinsky scheme |
| Vertical eddy viscosity | M-Y level-2.5 turbulent closure |
| Node, element, vertical layers | 49 906 grids, 6 uniform sigma layers |
| Open-boundary condition | sea-surface elevation time series from TPXO7.2 |

In Exp. 1, the model was run using the coastline data of 2003, as the observation data were collected during that year. This experiment was used as a reference run to examine the tidal dynamics in the bay. In Exps 2–4 (Exps 5–7), the coastline at the head of the Tie inlet was reduced (elevated) by 1, 2 and 3 m, respectively, to examine the impact of a bottom slope change in a tidal flat on the tidal dynamics in the bay. Similarly, the coastline around the Xihu inlet in Exps 8–10 was reduced, and that in Exps 11–13 was elevated, by 1, 2 and 3 m. The increase/decrease of the tidal flat areas in the Tie inlet was less than 0.000 6% (325.98 $m^2$)/0.000 9% (527.88 $m^2$) of those in the reference run. Similar ratios occurred at the Xihu inlet. Hence the variation of the areas of the tidal flats was ignored, as small changes of topography have very little impact on hydrodynamics (Zeng et al., 2011). These two inlets were chosen to conduct the numerical experiment because of their locations and vast tidal flat areas. When the coastline was elevated, the bathymetry of the coastline was increased, while the location of the coastline remained unchanged. The depth between the new coastline and the 5 m depth contour was linearly interpolated. The 5 m depth contour of the Tie inlet and Xihu inlet are shown in Figs 1d–e, respectively.

A detailed description of these numerical experiments is shown in Table 2. The coastlines which had been elevated or lowered are illustrated by dashed lines in Fig. 1a. Please note that Exps 4 and 7 were referred to Li et al. (2017). These two experiments remain here for consistency.

**Table 2.** Description of numerical experiments

| Experiment | Description |
|---|---|
| Exp. 1 | reference experiment using 2003 coastline |
| Exp. 2 | land boundary elevation around the Tie inlet reduced by 1 m |
| Exp. 3 | land boundary elevation around the Tie inlet reduced by 2 m |
| Exp. 4 | land boundary elevation around the Tie inlet reduced by 3 m |
| Exp. 5 | land boundary elevation around the Tie inlet increased by 1 m |
| Exp. 6 | land boundary elevation around the Tie inlet increased by 2 m |
| Exp. 7 | land boundary elevation around the Tie inlet increased by 3 m |
| Exp. 8 | land boundary elevation around the Xihu inlet reduced by 1 m |
| Exp. 9 | land boundary elevation around the Xihu inlet reduced by 2 m |
| Exp. 10 | land boundary elevation around the Xihu inlet reduced by 3 m |
| Exp. 11 | land boundary elevation around the Xihu inlet increased by 1 m |
| Exp. 12 | land boundary elevation around the Xihu inlet increased by 2 m |
| Exp. 13 | land boundary elevation around the Xihu inlet increased by 3 m |

### 2.3 *Calculation of tidal duration asymmetry and tidal energy*

If the duration of an ebb tide is shorter (longer) than that of the corresponding flood tide, and leads to a stronger ebb (flood) current, which is referred to as an ebb (flood) dominant system (Walton, 2002). The tidal duration asymmetry $\gamma_1$ can be calculated using the normalized sample skewness of a tidal-elevation time derivative $\frac{\partial \zeta}{\partial t} = \zeta'$ (Nidzieko, 2010):

$$\gamma_1 \equiv \frac{\mu_3}{\delta^3} = \frac{\frac{1}{T-1}\sum_{t=1}^{T}\left(\zeta_t' - \overline{\zeta'}\right)^3}{\left[\frac{1}{T-1}\sum_{t=1}^{T}\left(\zeta_t' - \overline{\zeta'}\right)^2\right]^{3/2}}, \tag{3}$$

where $\zeta$ is the sea-surface elevation (SSE), $\mu_3$ is the third sample moment about the mean and $\delta$ is the standard deviation (Emery and Thomson, 2001). The model was integrated for 31 days ($T$=31). The ebb-tide duration is shorter if $\gamma_1 < 0$, while the flood-tide duration is shorter if $\gamma_1 > 1$.

In an estuarine environment with tidal elevation and tidal currents generally 90° out of phase, the asymmetry $\gamma_1$ computed from a tidal elevation is similar to the asymmetry $\gamma_c$ calculated from currents in the absence of river runoff, stratification and bathymetry effects (Nidzieko, 2010), as is the case for Xiangshan Bay.

According to Song et al. (2011), $\gamma_1$ can also be calculated using amplitudes, frequencies and phases of all the components of astronomical tides:

$$\gamma_1 \approx \frac{\sum_{\omega_i+\omega_j=\omega_k}\frac{3}{2}a_i\omega_i a_j\omega_j a_k\omega_k \sin(\varphi_i+\varphi_j-\varphi_k) + \sum_{2\omega_i=\omega_j}\frac{3}{4}a_i^2\omega_i^2 a_j\omega_j \sin(2\varphi_i-\varphi_j)}{\left(\frac{1}{2}\sum_{i=1}^{N}a_i^2\omega_i^2\right)^{3/2}}, \tag{4}$$

where $a_i$, $\omega_i$ and $\varphi_i$ are the tidal amplitudes, frequencies and phases of the astronomical tides, respectively. In this study, the $M_2/M_4$ combination makes the most significant contribution. Other constituent combinations only play minor roles and can be neglected. If only these two constituents are considered, the tidal duration asymmetry $\gamma_1$ may be approximated by $\gamma_{M_2/M_4}$, according to Song et al. (2011):

$$\gamma_{M_2/M_4} = \frac{\frac{3}{2}a_{M_2}a_{M_4}\sin(2\varphi_{M_2}-\varphi_{M_4})}{\left[\frac{1}{2}\left(a_{M_2}^2+4a_{M_4}^2\right)\right]^{3/2}}. \tag{5}$$

The approximation $\gamma_{M_2/M_4}$ is used to analyze the controlling factors of tidal duration asymmetry in the bay.

Tidal duration asymmetry has an obvious fortnightly vari-

ation (Toublanc et al., 2015), which can be expressed as above (Nidzieko, 2010). To describe this fortnightly variation in duration asymmetry using the skewness method, Guo et al. (2016) followed the method that Nidzieko and Ralston (2012) and Song et al. (2011) promoted, to measure the fortnightly asymmetry using four $M_2$ tidal cycles (two lunar days):

$$\gamma_N(t) \approx \frac{\sum\limits_{\substack{|2\omega_i-\omega_j|<\varepsilon \\ i\neq j}}^{N} -\frac{3}{4}C(\omega_i,\omega_i,\omega_j) + \sum\limits_{\substack{|\omega_i|<\varepsilon \\ i\neq j}}^{N} -\frac{3}{2}D(\omega_i,\omega_j,\omega_j) + \sum\limits_{\substack{|\omega_i+\omega_j-\omega_k|<\varepsilon \\ i<j<k}}^{N} -\frac{3}{2}C(\omega_i,\omega_j,\omega_k) + \sum\limits_{\substack{|\omega_i-\omega_j+\omega_k|<\varepsilon \\ i<j<k}}^{N} -\frac{3}{2}D(\omega_i,\omega_j,\omega_k)}{\left[\sum\limits_{i=1}^{N}\frac{1}{2}B(\omega_i,\omega_i) + \sum\limits_{\substack{|\omega_i-\omega_j|<\varepsilon \\ i<j}}^{N} B(\omega_i,\omega_j)\right]^{3/2}}, \tag{6}$$

where $B(\omega_i,\omega_j) = a_i\omega_i a_j\omega_j \cos[(\omega_i-\omega_j)t-(\varphi_i-\varphi_j)]$, $C(\omega_i,\omega_j,\omega_k) = a_i\omega_i a_j\omega_j a_k\omega_k \sin[(\omega_i+\omega_j-\omega_k)t-(\varphi_i+\varphi_j-\varphi_k)]$ and $D(\omega_i,\omega_j,\omega_k) = a_i\omega_i a_j\omega_j a_k\omega_k \sin[(\omega_i-\omega_j+\omega_k)t-(\varphi_i-\varphi_j+\varphi_k)]$.

The meanings of $N$, $a$, $\omega$ and $\varphi$ are the same as above. Here, $\varepsilon$=4.8×10$^{-2}$ rad/h is chosen as the critical value between high- and low-frequency tides to produce a fortnightly variation. Note that the tidal constituents should be sorted from low to high in frequency before applying Eq. (6).

The equation for the fortnightly variation of the tidal asymmetry is proposed based on the method for the tidal duration asymmetry, to illustrate the temporal variability of the tidal duration asymmetry. The tidal duration asymmetry is calculated from the sea surface elevation data. The longer the integral time the better. Hence, one-month is used in this study to cover the spring-neap tidal cycle. The fortnightly variation of the tidal asymmetry is calculated using tidal elevation data in one or two tidal cycles. Hence, it is integrated in two days in this study.

The tidal energy flux ($\vec{E}_f$) over a unit width within one tidal cycle was calculated to analyze the tidal energy distribution in the bay (Song et al., 2011):

$$\vec{E}_f = \frac{1}{T}\int_0^T \rho D\left(g\zeta + \frac{1}{2}|\vec{v}|^2\right)\vec{v}\,\mathrm{d}t, \tag{7}$$

where $\rho$ is density of water, $\vec{v}$ is the eastward or northward velocity.

The energy dissipation due to bottom stresses was calculated by

$$W = \rho_w C_d |u_b| \vec{u}_b^2, \tag{8}$$

where $W$ is the tidal energy dissipation due to frictional drag (Zhu et al., 2016).

### 2.4 *Model calibration*

Hourly elevation data in November and December 2003 from the SOED were used to validate the principal tidal characteristics of the bay (Fig. 2a). The data were collected for about two consecutive months at three stations of Qiangjiao, Wushashan and Xize (Fig. 1a), starting from 7 November 2003 at one-hour intervals. These tidal data were used to calibrate the model results. Figure 2a shows the predicted elevation time series, which agree well with the field data from the three stations.

Table 3 shows the comparison of amplitudes and phases for the elevations of the major tidal constituents ($M_2$, $S_2$, $K_1$, $O_1$ and $K_2$) at Sta. Xize. Of these tidal constituents, $M_2$ is the predominant one. Table 3 demonstrates good agreement between the observed and simulated amplitudes and phases. The deviations of the model $M_2$ and $M_4$ amplitudes (phases) from those observed are 5.2% and 5.6% (3.9°and 10°), respectively.

Current velocity validation was conducted by comparing the observed and modeled current magnitudes and phases at the surface, middle and bottom levels at the three stations (figure not

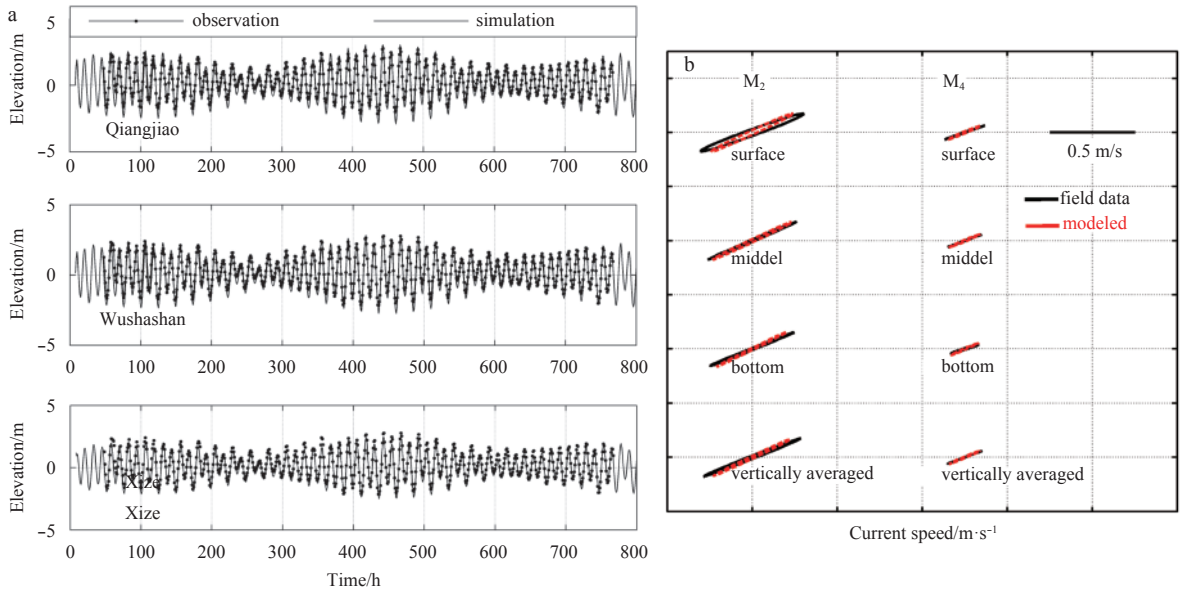


**Fig. 2.** Comparison between observed and modeled elevations (a) and current magnitudes and phases of the $M_2$ and $M_4$ tides (b). The *x*-axis is the hours from 00:00 on 7 November 2003.

**Table 3.** Comparison of model and observed tidal harmonic parameters at the Sta. Xize

| Main tidal constituent | Amplitude/m | | Amplitude deviation/% | Phase/(°) | | Phase deviation/(°) |
|---|---|---|---|---|---|---|
| | Observed | Model | | Observed | Model | |
| $O_1$ | 0.17 | 0.17 | 0 | 57.3 | 64.2 | 6.9 |
| $K_1$ | 0.33 | 0.27 | –15.1 | 94.1 | 99.6 | 5.5 |
| $M_2$ | 1.35 | 1.28 | –5.2 | 35.5 | 39.4 | 3.9 |
| $S_2$ | 0.59 | 0.49 | –16.9 | 77.9 | 74.7 | –3.2 |
| $M_4$ | 0.09 | 0.095 | 5.6 | 109.6 | 99.6 | –10 |

shown). The model trends in current speed and phase agreed well with the measurements, with average deviations of 0.1 m/s and 25° for current speed and direction at Sta. 2. The modeled magnitude and direction of the current ellipses of the $M_2$ and $M_4$ tides at Sta. 2 agreed well with the observed values, with deviations being less than 15% and 3° (Fig. 2b).

In conclusion, the model results show reasonably good agreement with the observed values, with acceptable errors, for elevations, currents, amplitudes and phases of the dominant tidal constituents of $M_2$ and $S_2$. Therefore, we believe that the model can be used to accurately simulate the tidal dynamics in the bay.

## 3 Results

In this section, the characteristics of tidal constituents in the bay are illustrated. The impacts on tidal dynamics by tidal flat's slope changes at the Tie inlet and Xihu inlet are elucidated.

### 3.1 *Modeled tides in the bay*

According to a harmonic analysis of sea level data from both field measurements and model results, the Xiangshan Bay is dominated by an $M_2$ tide and the main shallow-water tide is $M_4$. Hence, only $M_2$ and $M_4$ tides were analyzed in this study. The amplitude/phase of $M_2$ increased/delayed from the mouth (1.0 m/35°) to the head (1.8 m/45°) of the bay. The amplitude of $M_4$ increased by 0.28 m and the phase was delayed by 70° from the mouth to the head of the bay. The $M_2$ tidal current eclipses were rectilinear in the entire bay except at the bay mouth. The vertically averaged current speed of $M_2$ tide peaked at about 0.7 m/s. The maximum major axis of the $M_4$ tidal current was about 0.25 m/s (Fig. 3)

As the dominant astronomical and shallow-water tides are $M_2$ and $M_4$ tides, the tidal duration asymmetry in the bay can be measured by $\gamma_{M2/M4}$. Accumulated in one lunar month, tides in the inner (outer) bay were mainly ebb (flood) dominant (Fig. 4a, Eq. (5)). According to Eq. (6), the fortnightly asymmetry skewness, during spring and neap tides integral in two days, are negative/positive indicating ebb/flood dominant. The fortnightly asymmetry skewness during a spring tide is about three times of that during a neap tide (Figs 4b and c)

### 3.2 *Impacts on tides by tidal flat's slope change at the Tie inlet*

#### 3.2.1 *Tidal elevation*

In Exps 2–4, the coastline at the head of the Tie inlet was lowered gradually by 1, 2 and 3 m. The $M_2$ amplitude and phase (Figs 5a–c and a′–c′) in the bay was amplified/delayed gradually with the decrease of the tidal flat's slope, compared with the reference run. The largest increase/delay of about 0.05 m/1° appeared at the Tie inlet in Exp. 4 (Figs 5c and c′) when the coastline was lowered by 3 m around the inlet. This was due to the increase of tidal prism in the bay. When the coastline at the head of the Tie inlet was elevated by 1, 2 and 3 m, (Experiments 5–7), the $M_2$ amplitude and phase (Figs 5d–f and d′–f′) in the bay decreased and advanced by a similar magnitude with those in Exps 2–4. The largest decrease/advance of the $M_2$ amplitude/phase of about 0.05 m/1° occurred at the Tie inlet in Exp. 7 when the coastline around the inlet was elevated by 3 m. This was due to the decrease of tidal prism in the bay.

Figures 5g–l show the differences of $M_4$ tidal amplitude between Exps 2–4 and the reference run. The $M_4$ tidal amplitude changed by a similar magnitude, but in an opposite trend to that of the $M_2$ amplitude. According to previous studies (Li et al., 2017; Gao et al., 2014), the bottom friction had a greater dissipating effect than a generating effect on the $M_4$ tide. Advection only played a secondary role in generating the $M_4$ tide. Hence, the increased/decreased $M_4$ amplitude during an increase/reduced tidal flat's slope was due to reduced/increased bottom dissipation in the tidal flat zone. The $M_4$ tidal phase tended to be advanced in the entire bay in all the Exps 2–7.

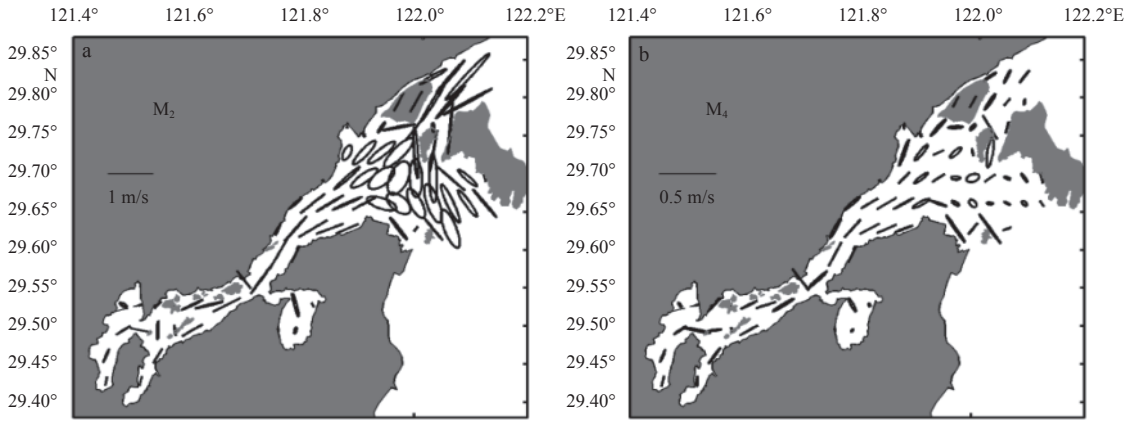


**Fig. 3.** Tidal current ellipses of $M_2$ tide (a) and $M_4$ tide (b).

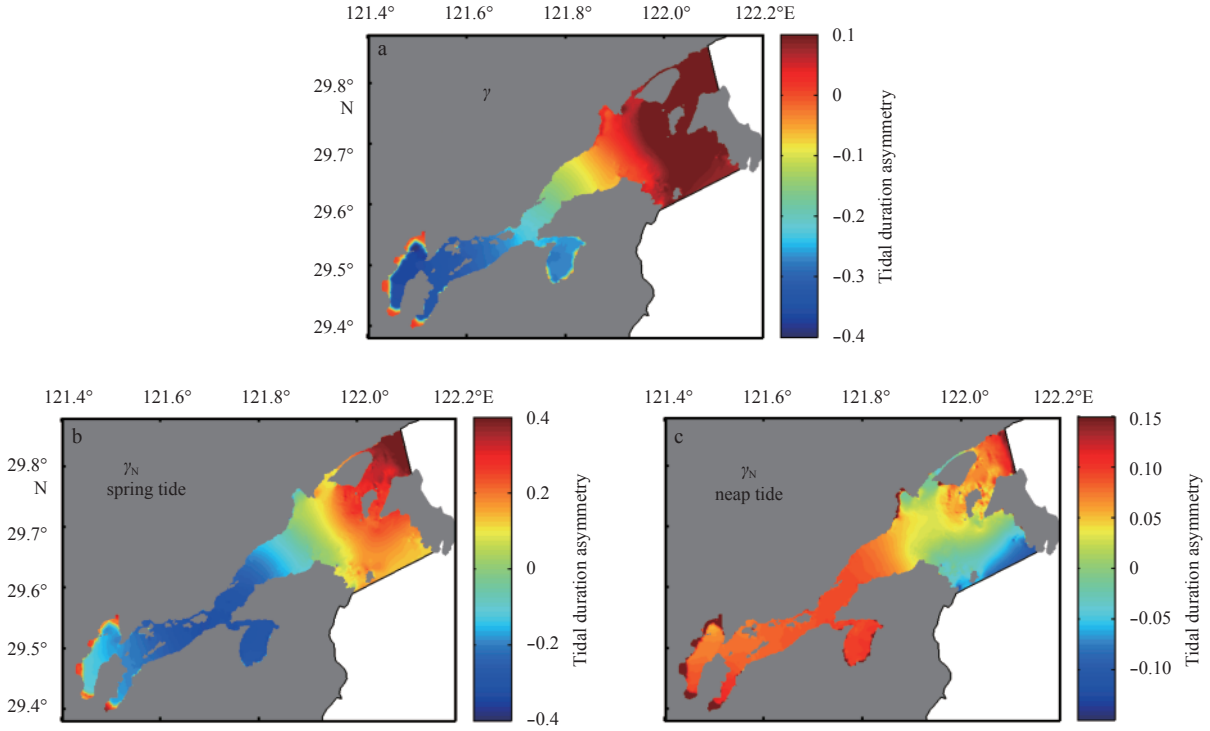


**Fig. 4.** Tidal duration asymmetry calculated by $M_2$ and $M_4$ tidal amplitudes and phases using Eq. (5) in one lunar month (a). Fortnightly asymmetry calculated using Eq. (6) averaged using two days during spring tide (b) and neap tide (c).

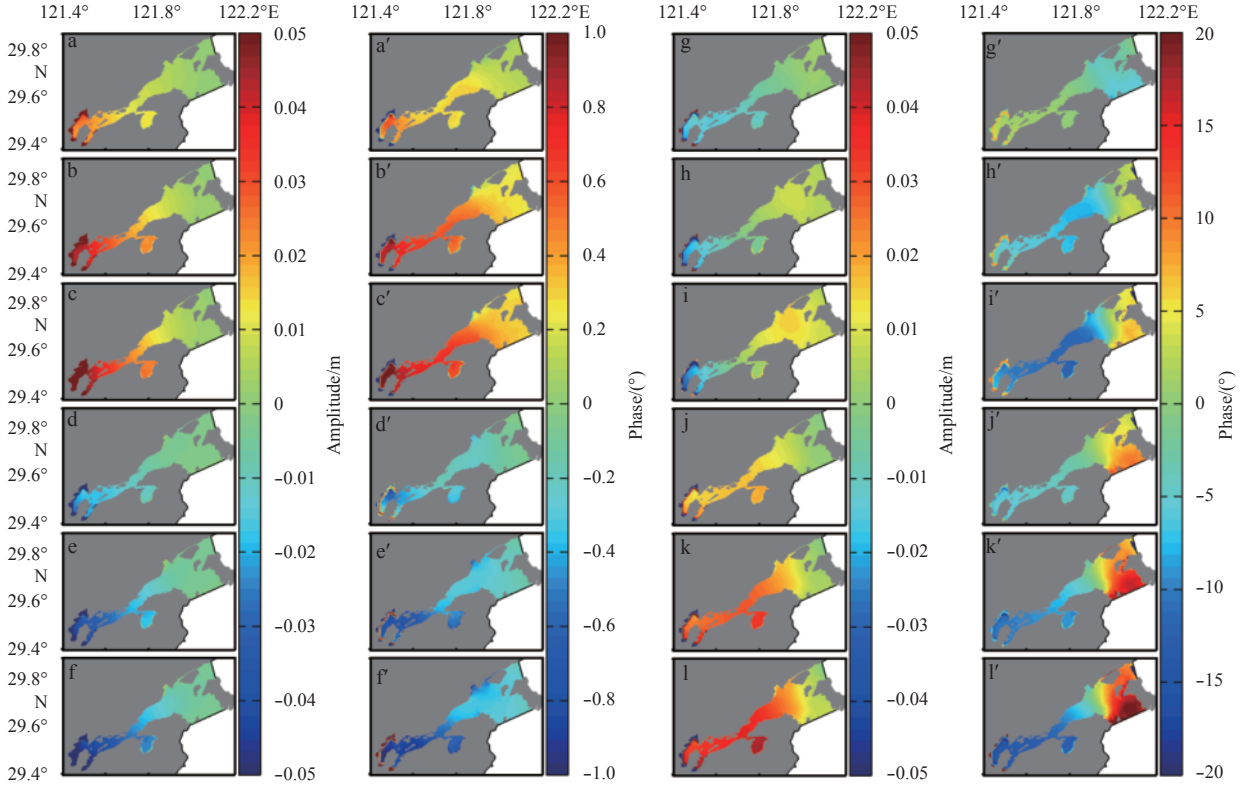


**Fig. 5.** Changes of $M_2$ tidal amplitude with land boundary elevation reduced by 1 m (a), 2 m (b) and 3 m (c), or increased by 1 m (d), 2 m (e) and 3 m (f) at the Tie inlet, compared with the reference experiment (Exp. 1). a′–f′ are same with a–f, but for $M_2$ phase; g–l and g′–l′ are for $M_4$ amplitude and phase.

3.2.2 *Tidal duration asymmetry produced by $M_2$ and $M_4$ tides*

Changes in $M_2$ and $M_4$ tidal amplitudes and phases caused changes of $M_2$ and $M_4$ in tidal duration asymmetry according to Eq. (5). Figures 6a–f show the tidal duration asymmetry differ-

ences between Exps 2–7 and the reference run. The asymmetry measured by the tidal elevation skewness tended to increase in the entire bay, indicating a decreased ebb dominance in the bay.

For the fortnightly variability (skewness by Eq. (6)) during the spring tides, the tidal duration asymmetry showed a similar trend, but with smaller magnitude (Figs 6a′–f′), with the tidal duration asymmetry skewness by Eqs (4) and (5) (Figs 6a–f), showing a decreased ebb dominance in the bay. During neap tides, the fortnightly asymmetry slightly decreased/increased in the bay in Exps 2–4/Exps 5–7 (Figs 6a"–c"/6d"–f"), indicating a decrease/increase of flood dominance in the bay, when the tidal flat's slope at the Tie inlet was reduced/increased.

### 3.3 *Impact on tides by a change in the tidal flat's slope at the Xihu inlet*

3.3.1 *Tidal elevation*

Unlike the Tie inlet, the Xihu inlet is located at the side bank of the Xiangshan Bay. The impact of the tidal flat's slope on tides was mostly constrained within the Xihu inlet (Exps 8–13, figure not shown). The local changes of $M_2$ amplitudes and phases were similar in trend, but smaller in magnitude than those when the tidal flat's slope at the Tie inlet was reduced or increased in Exps 2–7. The changes of $M_2$ and $M_4$ tidal amplitudes were both less than 20% of those in Exps 2–7. The changes of the $M_2/M_4$ phase were only 50%/25% of those in Exps 2–7.

The largest increase/decrease, of about 0.005 m/0.01 m, appeared in the Xihu inlet in Exp. 10/Exp. 13 where the coastline around the Xihu inlet was lowered/increased by 3 m. The $M_2$ and $M_4$ amplitude and phase in the main tidal channel remained almost the same.

3.3.2 *Tidal duration asymmetry produced by $M_2$ and $M_4$ tides*

If the tidal flat's slope around the Xihu inlet was reduced/increased (Figure not shown), the tidal duration asymmetry tended to slightly increase/decrease (to within 0.02, 5% of that in the reference run) in the entire bay, showing a decreased/increased ebb dominance. The magnitude of the changes of tidal duration asymmetry in Exps 8–13 for the Xihu inlet were less than those changes in Exps 2–7 (for the Tie inlet, Fig. 6).

The tidal duration asymmetry has fortnightly variability. During the spring tides it slightly increased/decreased (to within 0.04, 10% of that in the reference run) when the tidal flat's slope reduced/increased at the Xihu inlet, illustrating the dampened/amplified ebb dominance. During the neap tides, it remained almost the same as those in the reference run.

### 3.4 *Impact on tidal prism, residual current and tidal energy by tidal flat's slope change*

3.4.1 *Tidal prism*

Tidal prism in the bay was about $2.8\times10^9$ m$^3$/$0.6\times10^9$ m$^3$ during the spring/neap tides, respectively (Table 4) in the reference run. The Tie inlet and the Xihu inlet took 9% and 7% of the tidal prism in the bay, respectively. The variations of the tidal prism in the numerical experiments are illustrated as follows. Only the results from those experiments where the coastline increased/decreased by 3 m are presented.

During the spring tides, the tidal prism in the bay increased/decreased by 2.6%/3.0% in Exp. 4/Exp. 7, respectively, compared to that in the reference run. The reduced/increased (Exp. 4/Exp. 7) tidal flat's slope around the Tie inlet caused an increased/de-

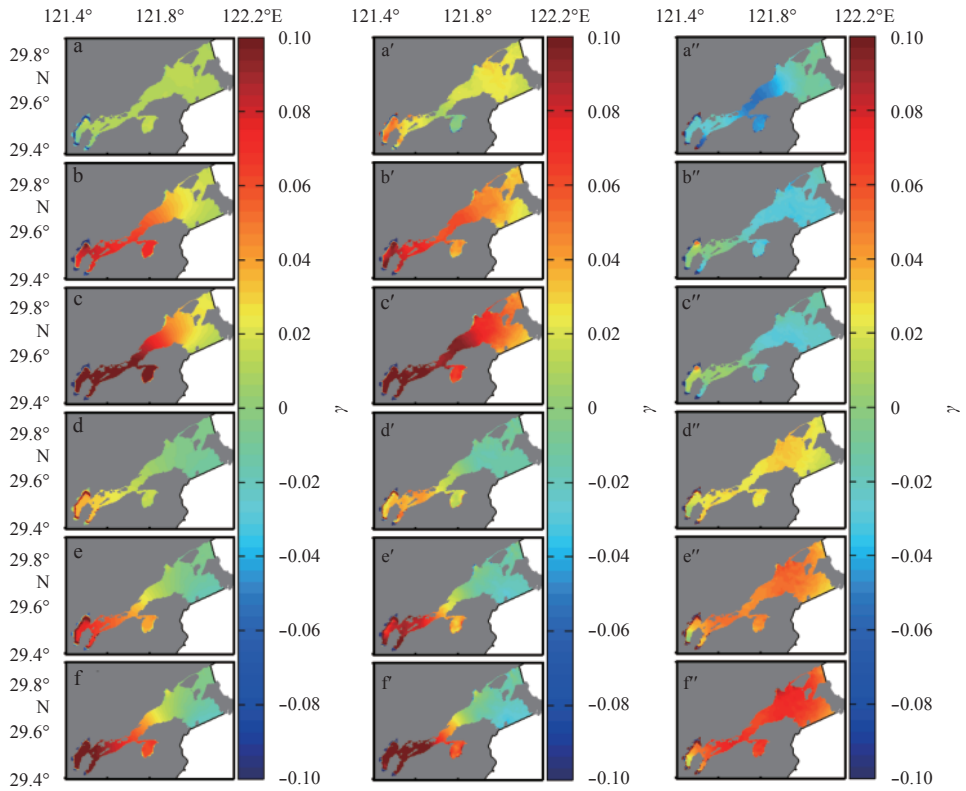


**Fig. 6.** Changes of tidal duration asymmetry skewness calculated by $M_2$ and $M_4$ tides with land boundary elevation reduced by 1 m (a), 2 m (b) and 3 m (c), or increased by 1 m (d), 2 m (e) and 3 m (f), at the Tie inlet, compared with the reference experiment (Exp. 1). The figures with prime and double prime are changes for fortnightly asymmetry skewness calculated using Eq. (6) integral using two days during spring and neap tide, respectively, compared with the reference experiment (Exp. 1).

**Table 4.** Differences of the tidal prism in the entire bay, the Tie inlet and the Xihu inlet during the spring and neap tides, respectively

| Experiment | Spring tides | | | | | |
|---|---|---|---|---|---|---|
| | The entire bay /$10^8$ m$^3$ | | Tie inlet /$10^8$ m$^3$ | | Xihu inlet /$10^8$ m$^3$ | |
| Exp. 4-Exp. 1 | 0.72 | 2.6% | 0.50 | 20.6% | 0.030 | 1.5% |
| Exp. 7-Exp. 1 | –0.84 | –3.0% | –0.57 | –23.3% | –0.001 4 | –0.07% |
| Exp. 10-Exp. 1 | 0.06 | 0.2% | –0.003 6 | –0.1% | 0.089 | 4.4% |
| Exp. 13-Exp. 1 | –0.2 | –0.7% | –0.012 | –0.5% | –0.17 | –8.4% |
| Experiment | Neap tides | | | | | |
| | The entire bay /$10^8$ m$^3$ | | Tie inlet /$10^8$ m$^3$ | | Xihu inlet /$10^8$ m$^3$ | |
| Exp. 4-Exp. 1 | 0.29 | 4.4% | 0.19 | 30.4% | 0.006 8 | 1.3% |
| Exp. 7-Exp. 1 | –0.16 | –2.4% | –0.15 | –24.1% | 0.002 3 | 0.4% |
| Exp. 10-Exp. 1 | 0.02 | 0.3% | 0.000 9 | 0.1% | 0.013 | 2.6% |
| Exp. 13-Exp. 1 | –0.09 | –1.4% | –0.004 5 | –0.7% | –0.063 | –12.0 |

creased tidal prism in both the Tie inlet (20.6%/23.3%) and the Xihu inlet (1.5%/0.07%). The magnitude of increase/decrease of tidal prism in the bay caused by the tidal flat's reduction/increase around the Xihu inlet (Exp. 10/Exp. 13) was 0.2%/0.7%, compared with the reference run. When the tidal flat's slope around the Tie inlet was increased/reduced (Exp. 4/Exp. 7), the variations of the tidal prism in the entire bay showed the same trend but had a different magnitude to that in the Tie inlet, and vice versa (Exp. 10/Exp. 13). An exception to this appeared in the Tie inlet in Exp. 10, when the tidal flat's slope around the Xihu inlet was reduced, the tidal prism increased in the Xihu inlet, while it reduced in the Tie inlet. A similar exception occurred at the Xihu inlet in Exp. 7 during the neap tides.

Variations of the tidal prism during the neap tides were similar to, but smaller than those during the spring tides.

3.4.2 *Residual current*

The residual current represents the net effects of tide-induced and baroclinically induced estuarine circulation, and is often used as an indicator of net water and sediment transport. The residual current in this study was calculated by averaging the tidal currents in a spring-neap tidal cycle to remove the periodical components.

The residual current in the reference model was seaward/landward in the main tidal channel/near the north and south banks, with a peak value of more than 0.15 m/s. A similar trend and magnitude occurred at the entrance of the Tie inlet. A large residual current appeared in the middle of the bay and in the shallow areas near the coastline. There was a divergent eddy inside the Xihu inlet, with a residual current speed of about 0.12 m/s.

If the coastline around the Tie inlet was reduced/increased by 3 m (Exps 4 and 7), the residual current in the entire bay was amplified/dampened, while the distribution pattern and the current direction were almost the same as the reference run (Figs 7a, b). The north part of the Tie inlet experienced the largest increase/decrease of about 0.02 m, when the tidal flat's slopes in the Tie inlet were reduced/increased. This was due to reduced/increased bottom dissipation in the tidal flat zone, when the tidal flat's slope was reduced/increased. The directions of residual currents in Exps 4 and 7 (Figs 7a′, b′, black arrows) were changed by less than 20° in the bay. The largest variation of more than 90° occurred at the Tie inlet and the Huangdun inlet.

Similar changes of trend and magnitude occurred in the residual current in the Xihu inlet, when the coastline around the inlet was reduced/increased (Exps 8 and 13, Figs 7c, d, c′, d′). However, the impacts on residual currents were constrained inside the Xihu inlet.

3.4.3 *Tidal energy flux and dissipation*

Tidal energy flux in the bay showed that the energy from the open sea propagated largely into Hangzhou Bay, and only a small part went into Xiangshan Bay. Inside the bay, the energy density was high (40 kW/m) in the main tidal channel in the middle of the bay.

The energy density increased/decreased (less than 5 kW/m) in the entire bay, when the tidal flat's slope around the Tie inlet decreased/increased (Exps 4 and 7) during the spring tide (Figs 8a–b), due to the increased/decreased tidal amplitude and current. A similar trend, but of smaller magnitude (less than 2 kW/m), occurred at the Xihu inlet due to tidal energy changes that decreased/increased the tidal flat's slope around the Xihu inlet.

Tidal energy loss was used to measure the energy available for the mixing of the water and to transport the sediment (Zhu et al., 2016). The work done by the bottom shear stress was mainly balanced by the energy dissipation occurring on the bottom layer. Hence, the bottom shear stress was calculated in the period of one lunar month, and compared between the experiments (Figs 8a′, d′). More/less energy (less than 0.02 W/m$^2$, Figs 8a′, b′) was dissipated in the bay when the tidal flat's slope decreased/increased around the Tie inlet. The impact of the changes in the tidal flat's slope at the Xihu inlet was local and small (less than 0.01 W/m$^2$, Figs 8c′, d′).

The changes in the dissipation pattern were in accordance with the variation of tidal current magnitude at the bottom level, as the bottom stress coefficient $C_d$ was constant in the entire bay.

## 4 Discussion

As illustrated in the results section, the change of the tidal flat's slope at the Tie inlet had a greater impact on tidal dynamics than the change at the Xihu inlet, because the amplitudes of $M_2$ and $M_4$ tides are the greatest at the head of a bay. Similar impacts of reclamation on $M_2$ and $M_4$ tides occurred at Jiaozhou Bay (Gao et al., 2014). The change in the tidal flat's slope at the Tie inlet caused greater variations in $M_2$ and $M_4$ tidal amplitudes (about five times) and phases (about two to four times) in the bay than the change at the Xihu inlet. The impact of the tidal flat's slope change at the Tie inlet on tidal duration asymmetry was more than four times as large as that at the Xihu inlet.

The changes of tidal flat's slope at the Xihu inlets caused greater local changes than far-field changes in terms of the tidal dynamics. This was due to the controlling effects of the bathymetry at the Xihu inlet, and, as a result, the effects of the change of the tidal flat's slope were mostly contained to the bay itself.

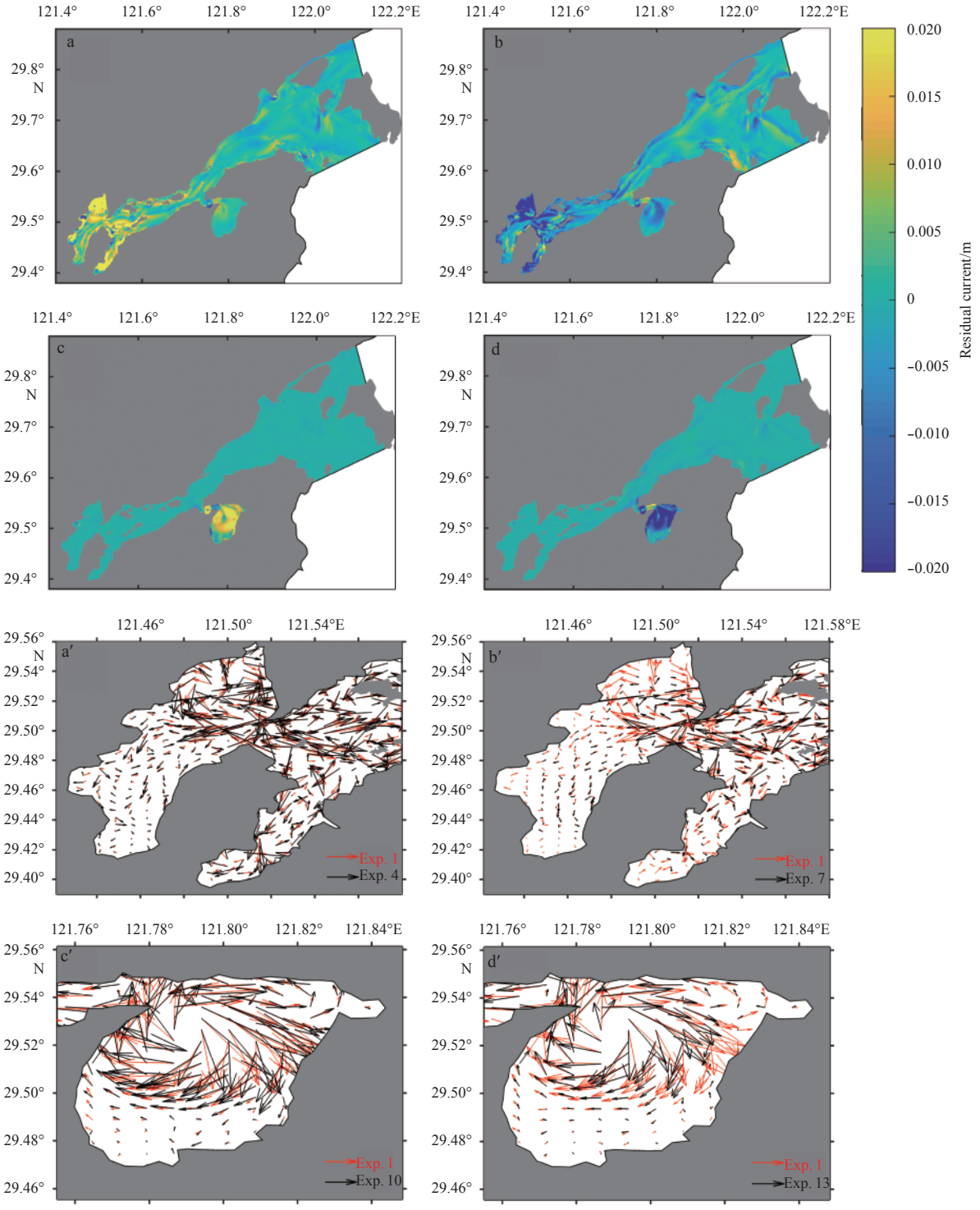


**Fig. 7.** Changes of residual currents with land boundary elevation reduced by 3 m (a), or increased by 3 m (b), at the Tie inlet, compared with the reference experiment (Exp. 1). Figures 7c and d are same with Figs 7a and b, but for Xihu inlet. Figures 7a′–d′ are same with Figs 7a-d, but for current direction. The red and black color is for the reference run and the comparative run, respectively.

Hence, the impacts of tidal flat's slope change at the Xihu inlet on tides and tidal duration asymmetry were more local than those at the Tie inlet. The impact of any engineering activities, such as land reclamation and sand mining, on tidal dynamics would be smaller at the Xihu inlet than at the Tie inlet.

The ebb dominance in the bay was amplified, when the tidal flat's slopes were increased in the Xihu inlet, which is opposite to the reduction of ebb dominance found in Exps 5–7 (where the tidal flat's slopes in the Tie inlet increased, Figs 6d–f). The same situation occurred to the fortnightly asymmetry during the spring tides with an increase in the tidal flat's slope at the Xihu inlet (figure not shown). The decrease of the water depth at the Xihu inlet would increase the ebb dominance, which is favorable to bottom erosion, and is better for navigational channel management.

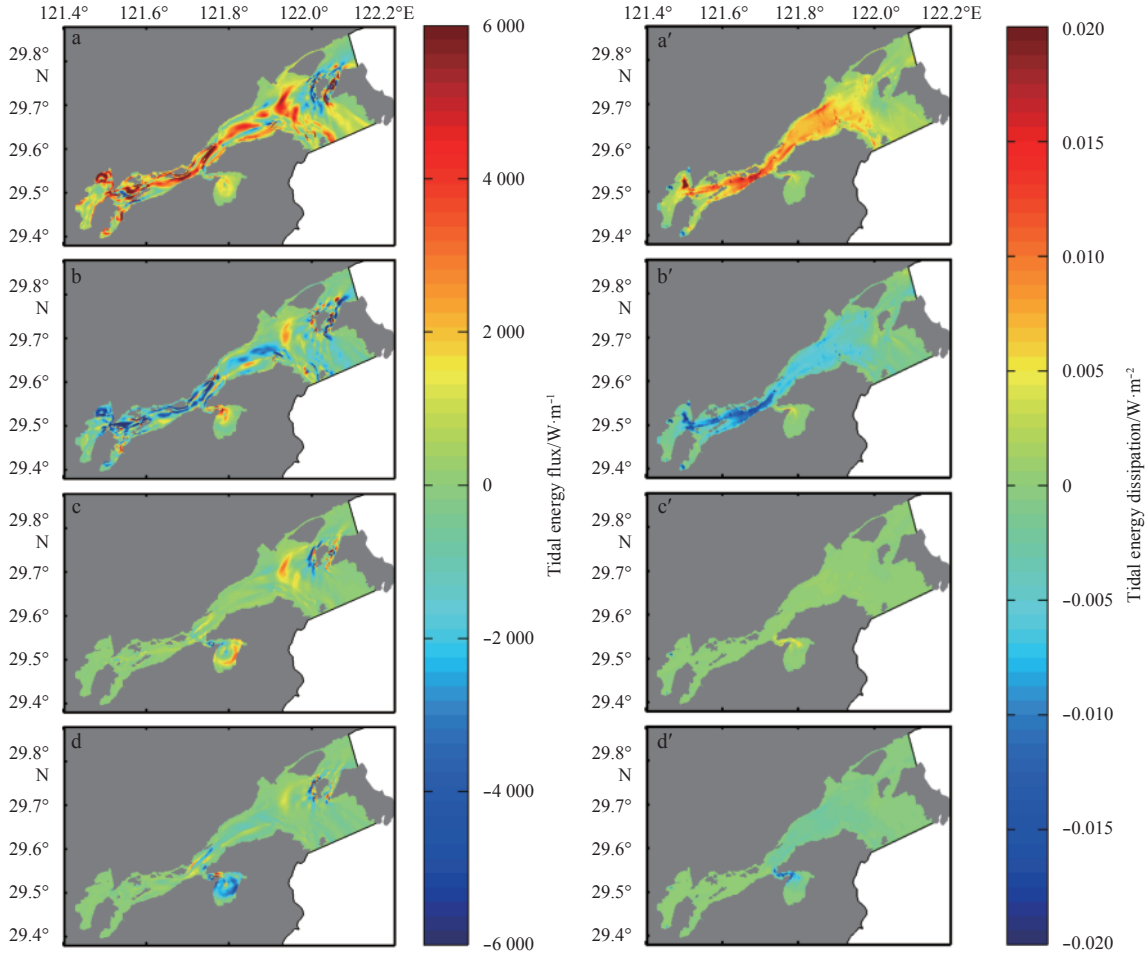


**Fig. 8.** Same as Fig. 7, except for tidal energy (a–d) flux and (a′–d′) dissipation.

## 5 Conclusions

In this study, the alteration of the tides in the Xiangshan Bay due to changes of tidal flat slopes was numerically investigated using the FVCOM model. Both the observed and modeled results indicate that the bay is semi-diurnal. The $M_2$ tide was predominant, with an amplitude of about 1.8 m at the head of the bay. The vertically-averaged current speed reached a maximum of about 0.7 m/s in the main tidal channel. The bay is ebb dominated, with a slight flood dominance occurring during neap tides.

According to the sensitivity tests, tidal flat's slopes impact tidal amplitude and phases through modulating tidal prism, bottom friction and advection processes. If the tidal flat's slopes at the Tie inlet were adjusted, the largest decrease/advance of the $M_2$ amplitude/phase that would occur at the Tie inlet would be about 0.05 m/1° if the coastline around the inlet was elevated by 3 m, due to a decreased tidal prism. The opposite trend would occur to the $M_4$ tide. Ebb dominance was dampened in the bay by both increased and reduced tidal flat's slopes at the Tie inlet. When the tidal flat's slopes at the Xihu inlet were adjusted, the local changes of $M_2$ amplitudes and phases were similar in trend, but smaller in magnitude than those at the Tie inlet. Ebb dominance was dampened/amplified in the bay by the reduced/increased tidal flat's slopes at the Xihu inlet.

The changes of the tidal flat's slope at the Tie inlet had a greater impact on tides, tidal asymmetry, residual current and tidal energy than those at the Xihu inlet. The impact of the tidal flat's slope changes on tides and tidal asymmetry was small and was confined locally to the Xihu inlet. The impact of the tidal flat's slope change at the Tie inlet on local tidal duration asymmetry, residual current and the tidal energy was more than two times than that at the Xihu inlet. The changes of the tidal flat's slope at the Tie inlet increased the tidal duration asymmetry, indicating a decreased ebb dominance in the bay. When there was a reduced/increased tidal flat's slope in the Tie inlet, the residual current was amplified/dampened by less than 0.02 m/s, the largest change of direction of the residual current was more than 90°, the tidal energy density was amplified/dampened by less than 5 kW/m, and more/less (<±0.02 W/m$^2$) tidal energy was dissipated. The change of tidal duration asymmetry would cause a decrease of seaward sediment transport and lead to an unstable coastal sediment dynamic.

## References

Azofra D, Martínez E, Jiménez E, et al. 2014. Comparison of the influence of biomass, solar-thermal and small hydraulic power on the Spanish electricity prices by means of artificial intelligence techniques. Applied Energy, 121: 28–37

Cai Weizhang, Chen Genxin, Ding Jinren. 1985. A discussion of the features of the tide and tidal current in the Xiangshan harbour and their cause of formation. Marine Science Bulletin (in Chinese), 4(3): 8–12

Chen Jian, Cai Feng. 2001. Coast evolution and sand transportation in east-southern Xiamen Island. Journal of Oceanography in Taiwan Strait (in Chinese), 20(5): 135–141

Chen Changsheng, Liu Hedong, Beardsley R C. 2003. An unstructured grid, finite-volume, three-dimensional, primitive equations ocean model: Application to coastal ocean and estuaries. Journal of Atmospheric and Oceanic Technology, 20(1): 159–186

Chen Wei, Su Jilan. 1999. A segmented tidal exchange model II. Application to the Xiangshan Estuary. Marine Environmental Science (in Chinese), 18(3): 7–10

Dallas K L, Barnard P L. 2011. Anthropogenic influences on shoreline and nearshore evolution in the San Francisco Bay coastal system. Estuarine, Coastal and Shelf Science, 92(1): 195–204

Dong Lixian, Su Jilan. 1999a. Tide response and tide wave distortion study in the Xiangshan Bay: II. Numerical modelling study in the Xiangshan Bay. Haiyang Xuebao (in Chinese), 21(2): 1–8

Dong Lixian, Su Jilan. 1999b. Tide response and wave distortion in Xiangshan Bay: I. Observation and analysis. Haiyang Xuebao (in Chinese), 21(1): 1–10

Emery W J, Thomson R E. 2001. Data Analysis Methods in Physical Oceanography. 2nd ed. Amsterdam: Elservier, 654

Franz G, Pinto L, Ascione I, et al. 2014. Modelling of cohesive sediment dynamics in tidal estuarine systems: Case study of Tagus estuary, Portugal. Estuarine, Coastal and Shelf Science, 151: 34–44

Friedrichs C T, Aubrey D G. 1994. Tidal propagation in strongly convergent channels. Journal of Geophysical Research, 99(C2): 3321–3336

Friedrichs C T, Madsen O S. 1992. Nonlinear diffusion of the tidal signal in frictionally dominated embayments. Journal of Geophysical Research, 97(C4): 5637–5650

Gao Linyu, Han Mukang. 2003. Some issues on littoral zone mining, coastal erosion and response strategies on northern coast of Shandong Peninsula. Research of Soil and Water Conservation (in Chinese), 10(3): 109–113

Gao Shu, Xie Qinchun, Feng Yingjun. 1990. Fine-grained sediment transport and sorting by tidal exchange in Xiangshan Bay, Zhejiang, China. Estuarine, Coastal and Shelf Science, 31(4): 397–409

Gao Guandong, Wang Xiaohua, Bao Xianwen. 2014. Land reclamation and its impact on tidal dynamics in Jiaozhou Bay, Qingdao, China. Estuarine, Coastal and Shelf Science, 151: 285–294

Gao Guandong, Wang Xiaohua, Bao Xianwen, et al. 2018. The impacts of land reclamation on suspended-sediment dynamics in Jiaozhou Bay, Qingdao, China. Estuarine, Coastal and Shelf Science, 206: 61-75

Guo Wenyun, Song Dehai, Wang Xiaohua, et al. 2016. Contributions of different tidal interactions to fortnightly variation in tidal duration asymmetry. Journal of Geophysical Research, 121(8): 5980–5994

Jiang Xuezhong, Lu Bing, He Yuhong. 2013. Response of the turbidity maximum zone to fluctuations in sediment discharge from river to estuary in the Changjiang Estuary (China). Estuarine, Coastal and Shelf Science, 131: 24–30

Jin Yongfu, Zheng Xijian, Li Jinduo. 2006. Effect of exploiting sand in the Qitou Estuary on the Zhujiajian's barrier beach. Marine Environmental Science (in Chinese), 25(3): 46–49

Ksanfomality L V, Breus T K, Oraevsky V N, et al. 1997. Investigations of Mercury using the "solar-Mercury observer" (INTERHELIOS). Advances in Space Research, 19(10): 1625–1628

Lee J G, Nishijima W, Mukai T, et al. 1998. Factors to determine the functions and structures in natural and constructed tidal flats. Water Research, 32(9): 2601–2606

Li Li, Guan Weibing, Hu Jiangyu, et al. 2018. Responses of water environment to tidal flat reduction in Xiangshan Bay: Part I hydrodynamics. Estuarine, Coastal and Shelf Science, 206:14-26

Li Li, Wang Xiaohua, Andutta F, et al. 2014. Effects of mangroves and tidal flats on suspended-sediment dynamics: Observational and numerical study of Darwin Harbour, Australia. Journal of Geophysical Research, 119(9): 5854–5873

Li Li, Wang Xiaohua, Williams D, et al. 2012. Numerical study of the effects of mangrove areas and tidal flats on tides: A case study of Darwin Harbour, Australia. Journal of Geophysical Research, 117(C6): C06011

Li Xiangyu, Zhu Jianrong, Yuan Rui, et al. 2016. Sediment trapping in the Changjiang Estuary: Observations in the North Passage over a spring-neap tidal cycle. Estuarine, Coastal and Shelf Science, 177: 8–19

Mellor G L, Yamada T. 1982. Development of a turbulence closure model for geophysical fluid problems. Reviews of Geophysics, 20(4): 851–875

Mishra D, Goyal P, Upadhyay A. 2015. Artificial intelligence based approach to forecast $PM_{2.5}$ during haze episodes: A case study of Delhi, India. Atmospheric Environment, 102: 239–248

Montalto F A, Steenhuis T S, Parlange J Y. 2006. The hydrology of Piermont Marsh, a reference for tidal marsh restoration in the Hudson River estuary, New York. Journal of Hydrology, 316(1-4): 108–128

Nidzieko N J. 2010. Tidal asymmetry in estuaries with mixed semidiurnal/diurnal tides. Journal of Geophysical Research, 115(C8): C08006

Nidzieko N J, Ralston D K. 2012. Tidal asymmetry and velocity skew over tidal flats and shallow channels within a macrotidal river delta. Journal of Geophysical Research, 117(C3): C03001

Niu Xiaojing, Yu Xiping. 2008. A practical model for the decay of random waves on muddy beaches. Journal of Hydrodynamics, Series B, 20(3): 288–292

Rees A B, Turner A, Comber S. 2014. Metal contamination of sediment by paint peeling from abandoned boats, with particular reference to lead. Science of the Total Environment, 494-495: 313–319

Seo Y, Kim S, Kisi O, et al. 2015. Daily water level forecasting using wavelet decomposition and artificial intelligence techniques. Journal of Hydrology, 520: 224–243

Shi B W, Yang S L, Wang Y P, et al. 2012. Relating accretion and erosion at an exposed tidal wetland to the bottom shear stress of combined current-wave action. Geomorphology, 138(1): 380–389

Smagorinsky J. 1963. General circulation experiments with the primitive equations: I. The basic experiment. Monthly Weather Review, 91(3): 99–164

Song Dehai, Wang Xiaohua, Kiss A E, et al. 2011. The contribution to tidal asymmetry by different combinations of tidal constituents. Journal of Geophysical Research, 116(C12): C12007

Song Dehai, Wang Xiaohua, Zhu Xueming, et al. 2013. Modeling studies of the far-field effects of tidal flat reclamation on tidal dynamics in the East China Seas. Estuarine, Coastal and Shelf Science, 133: 147–160

Toublanc F, Brenon I, Coulombier T, et al. 2015. Fortnightly tidal asymmetry inversions and perspectives on sediment dynamics in a macrotidal estuary (Charente, France). Continental Shelf Research, 94: 42–54

Trop T. 2017. An overview of the management policy for marine sand mining in Israeli Mediterranean shallow waters. Ocean & Coastal Management, 146: 77–88

Uścinowicz S, Jegliński W, Miotk-Szpiganowicz G, et al. 2014. Impact of sand extraction from the bottom of the southern Baltic Sea on the relief and sediments of the seabed. Oceanologia, 56(4): 857–880

Walton T. 2002. Tidal Velocity Asymmetry at Inlets. Vicksburg: US Army Corps of Engineers Press, 1-17

Wright L D, Boon J D, Xu J P, et al. 1992. The bottom boundary layer of the bay stem plains environment of lower Chesapeake bay. Estuarine, Coastal and Shelf Science, 35(1): 17–36

Xu Peng, Mao Xinyan, Jiang Wensheng, et al. 2014. A numerical study of tidal asymmetry: Preferable asymmetry of nonlinear mechanisms in Xiangshan Bay, East China Sea. Journal of Ocean University of China, 13(5): 733–741

Zeng Xiangming, Guan Weibing, Pan Chong. 2011. Cumulative influence of long term reclamation on hydrodynamics in the Xiangshangang Bay. Journal of Marine Sciences (in Chinese), 29(1): 73–83

Zhu Lei, He Qing, Shen Jian, et al. 2016. The influence of human activities on morphodynamics and alteration of sediment source and sink in the Changjiang Estuary. Geomorphology, 273: 52–62